

Ultrafast Coulomb explosion imaging of molecules and molecular clusters

Xiaokai Li(李孝开), Xitao Yu(余西涛), Pan Ma(马盼), Xinning Zhao(赵欣宁), Chuncheng Wang(王春成), Sizuo Luo(罗嗣佐)†, and Dajun Ding(丁大军)‡

Citation: Chin. Phys. B, 2022, 31 (**10**): 103304. DOI: 10.1088/1674-1056/ac89df
Journal homepage: http://cpb.iphy.ac.cn; http://iopscience.iop.org/cpb

What follows is a list of articles you may be interested in

Enhancement of isolated attosecond pulse generation by using long gas medium

Yueying Liang(梁玥瑛), Xinkui He(贺新奎), Kun Zhao(赵昆), Hao Teng(滕浩), and Zhiyi Wei(魏志义)
Chin. Phys. B, 2022, 31 (**4**): 043302. DOI: 10.1088/1674-1056/ac29a8

Geometric structure of N_2O^{q+} (q = 5, 6) studied by Ne^{8+} ion-induced Coulomb explosion imaging

Xi Zhao(赵曦), Xu Shan(单旭), Xiaolong Zhu(朱小龙), Lei Chen(陈磊), Zhenjie Shen(沈镇捷), Wentian Feng(冯文天), Dalong Guo(郭大龙), Dongmei Zhao(赵冬梅), Ruitian Zhang(张瑞田), Yong Gao(高永), Zhongkui Huang(黄忠魁), Shaofeng Zhang(张少锋), Xinwen Ma(马新文), and Xiangjun Chen(陈向军)
Chin. Phys. B, 2021, 30 (**11**): 113302. DOI: 10.1088/1674-1056/abff45

Comparative study of photoionization of atomic hydrogen by solving the one- and three-dimensional time-dependent Schrödinger equations

Shun Wang(王顺), Shahab Ullah Khan, Xiao-Qing Tian(田晓庆), Hui-Bin Sun(孙慧斌), and Wei-Chao Jiang(姜维超)
Chin. Phys. B, 2021, 30 (**8**): 083301. DOI: 10.1088/1674-1056/abea85

Review on non-dipole effects in ionization and harmonic generation of atoms and molecules

Mu-Xue Wang(王慕雪), Si-Ge Chen(陈思格), Hao Liang(梁昊), Liang-You Peng(彭良友)
Chin. Phys. B, 2020, 29 (**1**): 013302. DOI: 10.1088/1674-1056/ab5c10

Observation of the optical $X^2\Sigma_g^+$-$A^2\Pi_u$ coupling in N_2^+ lasing induced by intense laser field

Siqi Wang(王思琪), Yao Fu(付尧), Danwen Yao(姚丹雯), Shanming Chen(陈善铭), Wei Zhang(张维), Helong Li(李贺龙), Huailiang Xu(徐淮良)
Chin. Phys. B, 2019, 28 (**12**): 123301. DOI: 10.1088/1674-1056/ab54b1

TOPICAL REVIEW — Celebrating 30 Years of *Chinese Physics B*

Ultrafast Coulomb explosion imaging of molecules and molecular clusters

Xiaokai Li(李孝开), Xitao Yu(余西涛), Pan Ma(马盼), Xinning Zhao(赵欣宁), Chuncheng Wang(王春成), Sizuo Luo(罗嗣佐)[†], and Dajun Ding(丁大军)[‡]

Institute of Atomic and Molecular Physics, Jilin University, Changchun 130012, *China*

(Received 1 July 2022; revised manuscript received 15 August 2022; accepted manuscript online 16 August 2022)

Taking an image of their structure and a movie of their dynamics of small quantum systems have always been a dream of physicists and chemists. Laser-induced Coulomb explosion imaging (CEI) provides a great opportunity to make this dream a reality for small molecules or their aggregation — clusters. The method is unique for identifying the atomic locations with ångstrom spatial resolution and capturing the structural evolution with a femtosecond time scale, in particular for imaging transient state products. This review summarizes the determination of three-dimensional equilibrium geometry of molecules and molecular cluster system through the reconstruction from the fragments momenta, and also shows that the dissociation dynamics on the complex potential energy surface can be tracked in real-time with the ultrafast CEI (UCEI). Furthermore, the detailed measurement and analysis procedures of the CEI, theoretical methods, exemplary results, and future perspectives of the technique are described.

Keywords: Coulomb explosion imaging, molecular structure, molecular cluster, ultrafast dissociation dynamics

PACS: 33.20.Xx, 36.40.Mr, 82.53.Eb **DOI:** 10.1088/1674-1056/ac89df

1. Introduction

Promoting the ability to measure the structures of molecules and clusters and their evolution has always been a motivation of physicists and chemists.[1–5] Various advanced technologies have been developed for last thirty years, such as optical spectroscopy in microwave[6] and infrared regions,[7,8] photoelectron spectroscopy,[9] x-rays or electron diffraction.[2–4,10–13] These methods show great power in structural imaging in the atomic precision. With the rapid development of femtosecond laser technique, a class of imaging methods emerged for real-time "seeing" the structural evolution, *i.e.*, ultrafast x-ray or electron diffraction, Coulomb explosion imaging (CEI).[14–16] These new methods in femtosecond (fs) temporal and ångstrom (Å) spatial scale[17–23] in particular enable us to deeply understand the dynamics of small quantum systems and enrich the study to a large extent of ultrafast science community.

Among these imaging methods, CEI is a direct, real-time imaging for the structure and its evolution of small quantum systems in gaseous phase, typically in a molecular frame of reference. The Coulomb explosion (CE) phenomenon was firstly observed in the early time of the studies for the interaction between fast molecular ion beam and thin solid foils.[24–27] By the interaction, the valence electrons of the small molecular ion were rapidly striped furtherly. In the fast fragmentation during the CE, the molecular structure determined the velocity vectors of the repelled fragment ions, as shown in Fig. 1. In turn, exploiting the measured velocity vector of the fragments, CEI was introduced for reconstructing the static structure of the molecular ion.[14,26,28–30] Taking advantage of this principle, the first foil-induced CEI experiment was done by Vager *et al.* in 1989[14] in which the structure of small molecules such as positively charged methane ions CH_4^+ was successfully determined.[14,28]

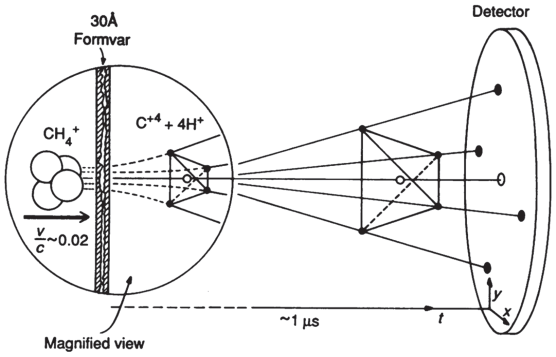


Fig. 1. Schematic diagram of the CEI by thin-foil experiment.[14]

Irradiation of molecules by a laser with a ps/fs pulse duration emerged as an alternative method to induce the Coulomb explosion around 1990 with the development of intense ultrafast lasers.[31–36] By contrast, the laser induced CE technique shows unique advantages in application of neutral molecules and clusters and together with detailed study of molecular dynamics through pump–probe method. Therefore, soon after that, laser-induced CEI was first demonstrated by

[†]Corresponding author. E-mail: luosz@jlu.edu.cn
[‡]Corresponding author. E-mail: dajund@jlu.edu.cn

© 2022 Chinese Physical Society and IOP Publishing Ltd

Stapelfeldt *et al.* in measuring the nuclear wavepacket structure and dynamics of I_2 molecule produced in an fs-pulsed laser field.[17,37] In this pump–probe measurement, a first fs laser pulse was used to launch a wavepacket in a dissociative excited state of the molecule, and a probe pulse was used to induce strong-field ionization and CE of the dissociating molecule. As shown in Fig. 2, increasing pump–probe delays correspond to increasing internuclear distances, thus the dissociation dynamics were mapped in the measured kinetic energy release (KER) spectrum.

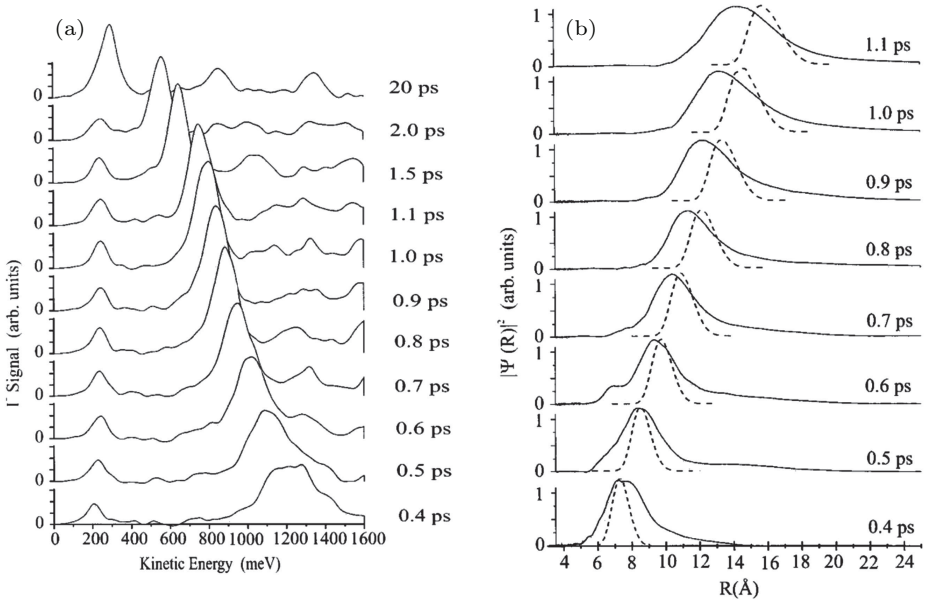


Fig. 2. Dissociative ionization dynamics in I_2 probed by CEI. (a) Kinetic energy release spectrum of I^+ and (b) square of the internuclear wave function of dissociative I_2 molecule measured at different times after excitation by the pump laser.[37]

Developing new detection method has promoted a significant progress of laser-induced CEI technique. In the early works on laser-induced CEI, a time-of-flight mass spectrometer was used generally, which confined it to the KER mapping of molecular structure and dynamics or the mass-resolved two-dimensional (2D) momentum imaging of molecular CE.[17] To determine structural information of a polyatomic molecule, the correlation between fragments is essential to be acquired. One solution is covariance mapping technique that identifies the correlation between directions/velocities of the fragments via a covariance analysis.[27,38] Recently, the angle-resolved covariance mapping with a 2D detector has been applied in imaging torsion of chiral molecules, identifying structural isomers and imaging structures of molecular dimer and trimer.[39] Another solution is coincidence momentum imaging technique by employing time- and position-sensitive detectors, such as, typically, cold-target recoil-ion momentum spectroscopy (COLTRIMS).[40–42] The technique implements a direct and differential measurement of three-dimensional (3D) momenta of all the fragment ions after the CE process. The earliest coincidence imaging focused on triatomic molecules (CS_2, D_2O and SO_2).[43–45] One of the employed apparatus is shown in Fig. 3. In these works, by reconstructing the bond length and bond angle of molecules before CE from the correlated momenta of fragments, it demonstrated the structural deformation in intense laser fields and sequential explosion process prior to the complete CE of molecule. Nowadays, through measuring all the five fragments of molecule (see Fig. 12),[15,46] or selectively detecting partial fragments (as shown in Fig. 4) to obtain clear momentum images depicting all the atoms within molecule,[47] which overcome the barrier for complete CEI of complex molecule, the stereo configurations of chiral or ring single molecules have been determined with coincident CEI.

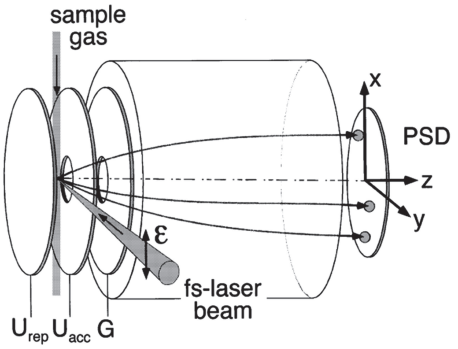


Fig. 3. Experimental apparatus for coincidence momentum imaging of CS_2 molecule. A velocity mapping configuration is employed with spaced repeller, accelerator, and ground electrodes. PSD: position-sensitive detector.[43]

Compared with other ultrafast imaging techniques such as ultrafast electron diffraction (UED) and ultrafast x-ray diffraction (UXD),[48] the femtosecond laser-induced CEI or ultrafast CEI has a better temporal resolution (up to several femtoseconds) with a spatial resolution of ångstrom and is compact and simple in device and easy to realize in method, as shown in Table 1.

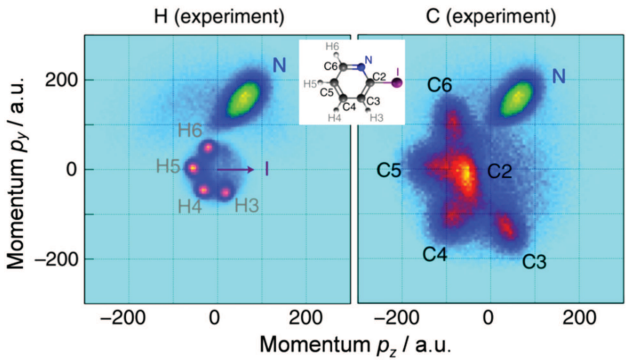


Fig. 4. Newton plots of N^+ and H^+ (left) and N^+ and C^+ (right) show the measured absolute momenta following CE of 2-iodopyridine (C_5H_4IN). For all the shots in which I^+, N^+, and at least one H^+ and one C^+ were detected, the coordinate frame is rotated such that the I^+ momentum points along the z axis.[47]

Table 1. Characteristics of typical ultrafast imaging techniques for gas-phase samples.

Technique	Temporal resolution	Spatial resolution	Setup
UCEI[17,23,57]	few to tens of fs	ångstrom	tabletop
UXD[48]	tens of fs	sub-ångstrom	large device
UED[48]	hundreds of fs	sub-ångstrom	large device

In particular, it is beneficial to image the transient structures of molecules and clusters in a table-top apparatus. The technique has generally been applied in structure-sensitive and dynamics studies for molecules and molecular clusters, including quantitative characterization of alignment and orientation for various molecules,[39,49] determination of the absolute configuration of chiral molecules,[15,16] identification of structural isomers,[50,51] time-resolved imaging of intramolecular processes,[52] and visualizing geometry and intermolecular interaction of weakly bound molecular cluster.[53–56]

2. The basic of laser induced CEI

The basic idea of CEI can be simply described as a process that a multiple charged molecule/cluster occurs a rapid break-up due to the strongly repulsive force from the Coulombic interaction among each charged sites within the molecule/cluster. For igniting a CE, multiple electrons are removed from molecule by absorbing enough amount of energy, either by charged particle (electron/ion) collision[58–61] or by photon (x-ray irradiation/intense laser).[17,47,62–74] This process need to be fast enough for ensuring the nuclei within the molecular frame do not move. The system, in the quantum view, are populated in the high-lying repulsive potential energy surfaces of its cation after several electrons releasing, and the relative momenta of the charged fragments produced preserve the information of the initial structure of the molecular system when the axial recoil approximation[75–77] holds due to the ultrafast ionization of the system, as shown in Fig. 5. Then the structural parameters of molecules and clusters can be readily reconstructed by the fully coincidently measured momenta of these fragments with the help of solving the classical Newtonian laws of motion within a Coulomb potential.[77]

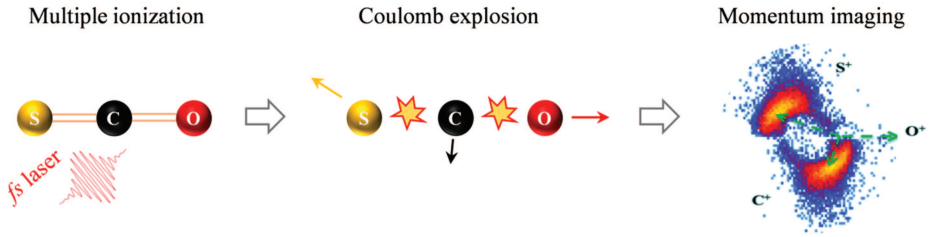


Fig. 5. Schematic diagram of laser-induced CEI of molecules. After strong-field laser-induced multiple ionization, the resulted multiple charged cation undergoes a rapid dissociation, *i.e.*, Coulomb explosion, due to strong Coulomb repulsions. The structure of molecules or molecular clusters can be reconstructed from the coincidently measured momenta of fragments.

The accuracy of reconstructed molecular structure by CEI mainly depends on the configurational change during multiple ionization and the validity of the Coulomb approximation. For laser-induced CEI, the obtained structure is actually the instantaneous structure just before the CE, thus the possible deformation of configuration from neutral to high-charge states has a remarkable influence on the accuracy, and few-fs pulses and heavy nuclei are more beneficial for experiment. If pulses with tens of fs duration are used in measurement, molecular vibrations mainly contribute to the motions involved in molecular configurational changes on this time scale, where the stretching of bond length is significant in longer pulses while the change of bond angle is small.[78] In addition, bending motion of molecules induced by laser-modified potential energy surface has little effect on the accuracy, because its time scale is much larger than that of stretching motion, usually on the order of hundreds of fs or even ps.[79,80] Another important assumption is Coulomb approximation that describes the interaction between fragments by only Coulomb repulsion. However, due to non-Coulombic interactions between the fragments, it may results in an overestimated bond length in comparison to the actual situation. For example, the bond length of CO_2 obtained with using the *ab initio* potential is 1.1 Å, which is basically consistent with the neutral result of 1.16 Å, while the bond length obtained by using the Coulomb potential is 1.7 Å.[63] This deviation can be reduced by using *ab initio* potential for reconstruction or by fast ionization to higher charge states to induce the CE. By the way, in spite of the confinements in

acquiring precise structure parameter of molecule, CEI has played an important role in fs-resolved real-time imaging of molecular dynamics and chemical reaction due to its high temporal resolution.

The structural imaging based on strong-field ionization triggered CE also relies on the understanding of the process of ionization and fragmentation.[57,63,81–83] In a study of wavelength-dependent CE of D_2, it shows that the measured internuclear separation between two D atoms increases from around 0.88 Å to 1.11 Å before CE when the time delay of recollision increases about 2.5 fs. Furthermore, the most probable bond distance extracted from measurement can change when the duration of laser pulse becomes longer, and this effect will diminish when the laser duration is small because the nuclei do not have enough time to stretch. Some evidences also demonstrate the effect of the polarization of laser pulse on the CE of molecules.[67,84,85] When linearly polarized (LP) and circularly polarized (CP) laser being used, the reorientation during CE and geometry modification shows different behaviors.

Importantly, the study on fragmentation mechanisms of ultrafast ionization and dissociation of molecules in turn pursues the ability of CEI. Generally, concerted and sequential fragmentation processes of molecules can occur after multiple ionization,[63,81] in which, however, only the fragment momenta from the concerted process meets the recoil approximation and can be used to reconstruct the molecular structures. Fortunately, the studies of molecular dynamics can be performed in the UCEI process by combining with a femtosecond laser pump–probe method. For example, the vibration and bond-breaking of molecules were tracked in real-time by a wide variety of research groups,[18–23,86] resulting in the feasibility in the fs time-resolved studies on conical intersection of different electronic states,[87] proton migration (H_3^+ formation), and roaming dynamics of molecules as well.[52,88–90]

3. Experimental method and calculation procedure

In a CE process, the measurement of the momenta of the fragments from molecular explosion has been achieved in different techniques: in early time such as time-of-flight (TOF) mass spectrometer or velocity-map imaging (VMI) setup were employed,[40,57,91,92] and nowadays coincidence momentum imaging setup,[43,45] especially COLTRIMS, was in general used for acquiring the 3D momenta of fragments coincidently.[41,42] In the measurement of laser induced CE by COLTRIMS, as shown in Fig. 6, multi-charged molecular ions are produced by femtosecond laser pulses focused on a supersonic molecular beam. Normally, the field of the laser pulses can reach a peak intensity ranging from 10^{14} W/cm^2 to 10^{18} W/cm^2 for the laser duration of several to tens of fs. With a relatively weak homogeneous electric field along z axis, the produced ions are projected onto the delay-line detector which has a good position detection ability and a rapid time response of sub-nanosecond. In this case 3D momenta of the ions can be calculated from their position on the detector (x, y) and time of flight (t_{TOF})

$$P_x = xm/t_{\mathrm{TOF}}, \tag{1}$$

$$P_y = ym/t_{\mathrm{TOF}}, \tag{2}$$

$$P_z = -\frac{1}{2}qEt_{\mathrm{TOF}} + mL/t_{\mathrm{TOF}}, \tag{3}$$

where m is the ion mass, q the charge, E the electric field strength, and L the length of the flight. In the meanwhile, the event count rate per laser shot is always limited to less than 1 to satisfy the basic coincidence condition for the case of molecules, thus a long acquisition time is required for multi-body coincidence measurement, especially for cluster samples whose proportion is small in the molecular beam, under the proper momentum conservation conditions for selecting the correct fragment signals from the same molecule/cluster.

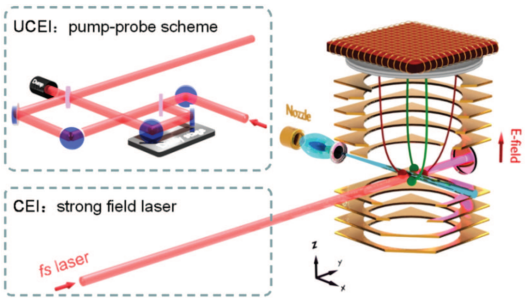


Fig. 6. Schematic diagram of the strong field CE experimental setup. The COLTRIMS can coincidently measure the full 3D momenta of fragments from strong field laser-induced CE, which are used to reconstruct molecular structure. The UCEI of molecular dynamics can be performed based on pump–probe scheme.

The simulation of the CE can be performed both in *ab initio* and classical trajectory methods, whose difference lies in how to calculate the potential energy surfaces (PESs) and the nonadiabatic transition between the surfaces.[14,15,75–77] The nuclear movements during CE are performed by solving Newton's equation of motion

$$\sum_{j=1,j\neq i}^{4} \frac{q_i q_j}{|\boldsymbol{r}_{ij}|^3}\boldsymbol{r}_{ij} = m_i\ddot{\boldsymbol{r}}_i \quad (i=1,2,3), \tag{4}$$

where m_i, q_i are the mass and charge of the i-th fragment ion, respectively, $\ddot{\boldsymbol{r}}_i$ is the second derivative of the position vector of the i-th ion, and $\boldsymbol{r}_{ij}$ is the position vector from the j-th to i-th ion. In the case of *ab initio* trajectory simulation, the PESs are calculated with quantum chemical methods.[76,77] Thus, the initial velocity (starts with zero) of the ion is accumulated from its moving on the previous PESs, accelerated (a derivative of the PES), and its final velocity is obtained from the time step as inputs for Newton's equations of motion to predict the distance traveled within the step. This calculation is repeated and all these outputs would be put to the next iteration of the

loop until the movement is ended when the ions are far away from each other or reach a defined evolution time.

Moreover, the nonadiabatic transition between different PESs can be calculated by a nonadiabatic *ab initio* molecular dynamics or using a semiclassical Landau–Zener surface hopping method,[22] but, it is very difficult to carry out for a system with complex structure or lying at a high charge state.[76,77] To solve those problems, a classical CE trajectory simulation must be carried out, in order to provide detailed information on the dissociation dynamics of the system, together with the help of a genetic algorithm with setting the goodness parameter

$$\eta = \sum_{i=1}^{N} |p_i^{\mathrm{e}} - p_i^{\mathrm{s}}| + \sum_{j>i}^{N} |\Delta p_{ij}^{\mathrm{e}} - \Delta p_{ij}^{\mathrm{s}}| \tag{5}$$

to reconstruct the structural parameters of the system.

Taking a four-body CE of the cluster as an example, figure 7 shows the flow of structure reconstruction in coordinate space according to the measured fragment momenta. The momenta of four fragments from the classical CE trajectory simulation are compared with the measured ones by varying the initial structure using a genetic algorithm. The correct structures are saved when the goodness parameter η meets the predefined requirement. Normally, this goodness parameter is set lower than 1% of the magnitude of the momenta of the fragments (about 200 a.u. here), and those structures with higher goodness parameters are required to be reconstructed again.

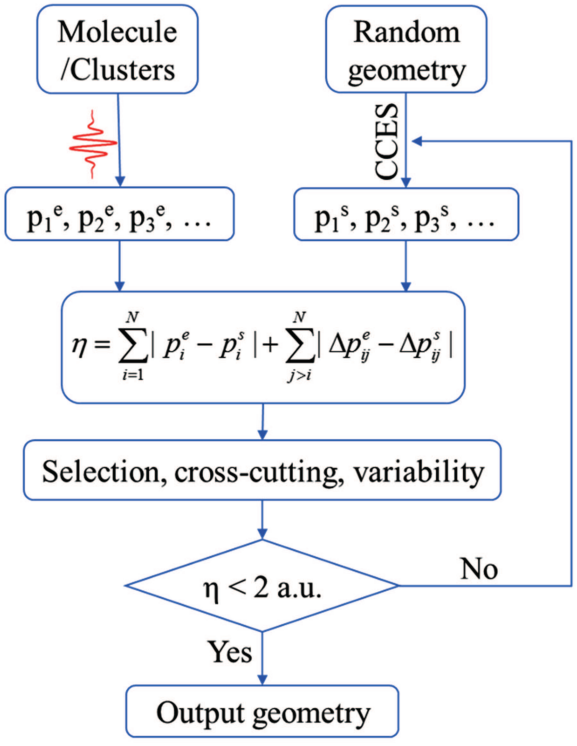


Fig. 7. Flow chart of structural reconstruction based on the classical CE simulation (CCES).

4. Imaging the structures of molecules and clusters directly by CEI

The CE dynamics of molecules in the strong laser field not only enriches the understanding of laser–matter interaction but also prompts a lot of interesting applications, including structural imaging of small molecules, chiral molecules, and molecular clusters.

4.1. CEI for small molecules and chiral molecules

In practice, it is not a easy task for the realization of a molecular CEI. As mentioned above, the molecular structural imaging based on intense laser-induced CE relies on the understanding and analysis of the process of molecular ionization and fragmentation.[57,63,81–83] Since sequential and nonsequential ionization of molecule have different time scales for multiple electron emissions, from tens of fs to sub-fs, it may lead to a discrepancy of extracted structural parameters even the CE occurs in the same charge states of the molecule.[57,83] At the same time, when molecular bond length increases over a critical distance, the molecule can ionize more efficiently in the strong laser field, known as charge resonance enhanced ionization.[65,93] Therefore, the responses of molecule dynamics during ionization and dissociation to the strong laser fields influence largely the obtained final momenta of fragments and also the reconstructed molecular parameters.

In the analysis of fragmentation dynamics of molecule, Newton diagram and Dalitz plot are usually introduced to understand the relations of ion momentum vector and correlation of energy of three-body CE. As shown in Fig. 8(a), in the Newton diagram, the measured momentum vectors of all the three fragments are rotated into a plane while keeping their relative angles unchanged. Momentum vector of one of the fragments is rotated to the positive half of horizontal axis, and those of the other two fragments are rotated to the upper and lower half of the plane, respectively. Then their absolute values are normalized by the magnitude of the first ion. The Newton diagram aims to analyze the statistical characteristics of the relative angles of momentum vectors of fragments in the same mass center system and distinguish the concerted or sequential fragmentation. For example, in the Newton diagram of the laser induced three-body CE channel $C^+ + O^+ + S^+$ of OCS molecules in Fig. 8(a), the concentrated crescent distribution is caused by a simultaneous CE of the three fragments, *i.e.*, a nonsequential or concerted fragmentation, while the annular distribution is caused by rotation of intermediate state during the dissociation process, indicating a step-by-step sequential fragmentation. The correlation of fragment momenta through the sequential fragmentation is schematically shown in Fig. 8(b). In the Dalitz plot, the horizontal axis is set as $(\varepsilon_2 - \varepsilon_3)/(\sqrt{3}W)$ and the vertical axis $\varepsilon_1/W - 1/3$, where ε_1, ε_2, and ε_3 denote the measured kinetic energy of the ions and

W is their energy sum. By analyzing the energy correlation of the three fragments in the Dalitz plot, with reference to the simulated distribution of fragmental momentum vectors as shown in Fig. 8(d), the changes of bond length and bond angle can be illustrated intuitively and the mechanism of dissociation and deformation of molecular configuration can be further distinguished. For example, the involved processes during fragmentation in black, red and green circular areas in Fig. 8(d) are determined as direct CE, bending of molecular bond and asymmetric stretching of molecular bond, respectively. The green circular area also corresponds to the annular part in Fig. 8(a), thus, it means a sequential dissociation channel caused by asymmetric stretching of molecular bond. By analysing separated regions in the Newton and Dalitz plots, it is helpful for distinguishing distinct fragmentation regime and improving the accuracy of CEI.

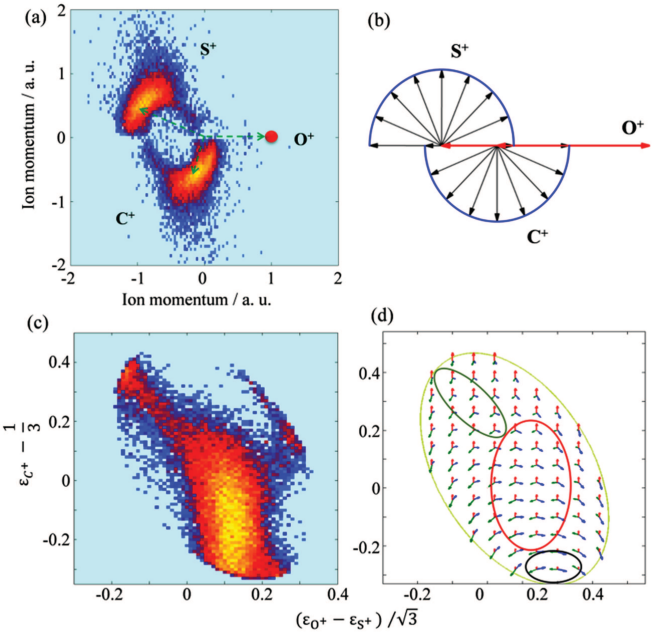


Fig. 8. (a) Newton diagram of the coincidently measured fragments of OCS^{3+}, the red dot represents the normalized mometum of oxygen ions along the x axis. (b) Schematic diagram of the momentum vector distribution of the three ions. (c) Dalitz diagram for the same CE channel, the ordinate represents the energy of carbon ion and the abscissa represents the energy difference between oxygen ion and sulfur ion. (d) Simulated momentum vectors of the three ions in the Dalitz distribution.

It is found that the duration, intensity, polarization, and wavelength of laser pulse have important effects on the CEI of polyatomic molecules.[67,84,85] For example, molecule may undergo an ultrafast deformation of geometrical structure in strong laser field and it is related to the pulse duration.[78,93] Figure 9 shows the reconstructed distribution of bond angles of several typical triatomic molecules from coincidently measured three-body CE in $\sim$ 40-fs laser fields, and the extracted bond angles and bond lengths from experiment are comparatively present with the corresponding theoretical values from equilibrium molecular geometry in Table 2. It shows larger deviations for bond length than bond angle between the experiment and theory, which indicates that, during the multiple ionization process, a configuration deformation happens and it mainly results from the stretching of bond length rather than the change of bond angle. Polarization of laser fields also have an influence on molecular CE.[67,94] As an example, the reorientation and geometry modification of OCS molecule during CE show different behaviors when using linearly and circularly polarized laser, which is indicated by the KER spectrum of CEs from various charge states, as shown in Fig. 10. It is found that the KER induced by the LP laser is higher than that obtained from the CP laser, especially when the charge state is higher than 5. This is attributed to the stronger molecular bending in highly charged states before three-body CE in the CP laser fields.[67]

Table 2. Bond angles and lengths of molecules extracted from CEI measurement and calculated by theory. The theory values correspond to an equilibrium molecular geometry and experimental results are extracted from three-body CE of triply-charged ions.

	Bond angle (°)		Bond length (Å)	
	Experiment	Theory	Theory	Experiment
OCS	165	172	1.16/1.56	1.96/2.13
N_2O	165	174	1.13/1.19	1.65/1.67
NO_2	128	134	1.2	1.7
SO_2	100	119	1.43	2.3

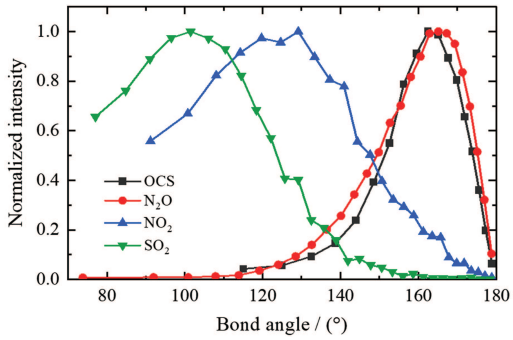


Fig. 9. Molecular bond angles reconstructed from measured momenta vector of three-body CE-induced fragments.

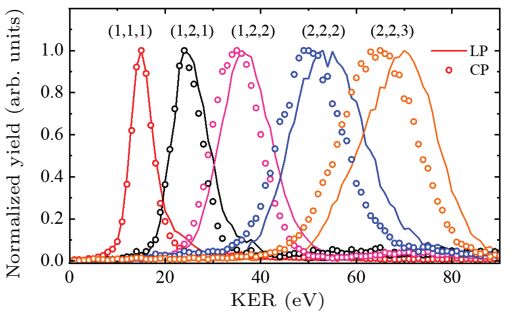


Fig. 10. Total KER spectra of CE channels of OCS in the LP and CP laser fields, (m, n, q) represents the charges of fragments (O^{m+}, C^{n+}, S^{q+}).[67]

On the other hand, CEI is helpful to understand the mechanism of laser-induced ionization and dissociation. Through CEI, it is observed that the dissociative ionization dynamics

strongly relies on the C–S or C–O bond breakage of asymmetric molecules OCS.[68] With measuring the evolution of KER distributions of different two-body CE channels of C–S and C–O bond breakages, and the nuclear distances between fragments of ions at the time of the Coulomb explosion were calculated. The value of bond length R scarcely changes (approximately 3.3 Å) for the C–S bond breaking, whereas it increases for the C–O bond breakage from 2.3 Å to 3.2 Å as the parent charge state increases from 2 to 4. With the help of the potential–energy curves (PEC) obtained from the multistate density-functional-theory method in Fig. 11, the enhanced multiple ionization proceed through field ionization to the higher charge states at the same position of critical distance R_c, which dissociate along all the PECs of Coulombic repulsion states. The CE along the C–O bond breakage must overcome a potential barrier step by step, which process is named as ladder-climbing-type sequential ionization. Thus, through CEI of laser induced dissociative ionization, the ionization mechanism of asymmetric molecules is shown to be determined by the bond breaking mode.

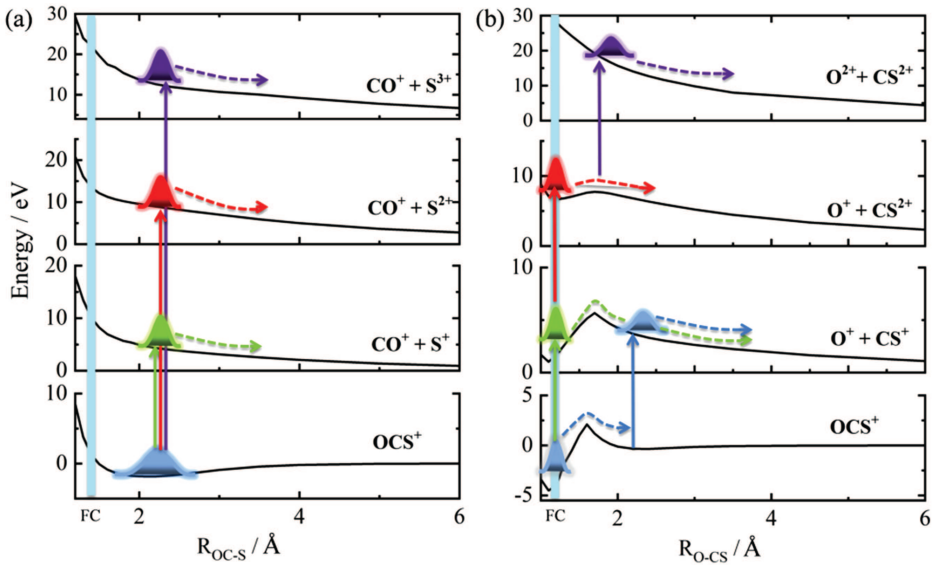


Fig. 11. Mechanism of dissociative ionization of OCS on molecular potential–energy curves when (a) stretching along the C–S bond, (b) stretching along the C–O bond.[68]

Chiral molecule is a class of molecules having an enantiomer with non-identical mirror stereo configurations.[15,16] The identification of molecular chirality is particularly meaningful in chemistry, biology, and medicine. Recently, the CEI has been successfully demonstrated in determining the absolute stereo configuration of chiral molecules CHBrClF and $C_2D_2H_2O$.[15,16] Figure 12 gives the measured linear momenta in fivefold fragmentation (C^+, H^+, Br^+, Cl^+, F^+) of CHBrClF enantiomers from coincidence measurement after laser-induced ionization of the molecules.[15] The obtained CEI clearly shows two mirrored enantiomers well and directly resolved. However, the five-body coincidence measurement requires not only a high detection efficiency but also an increased laser repetition rate for enough statistics of the data collected. Several studies have also indicated that combining with laser-induced alignment the CEI can further identify the absolute configuration of chiral molecules more efficiently for complex molecules. Christensen *et al.* have successfully demonstrated this method in determining the absolute configuration of $C_{13}H_5Br_2F_2N$ molecule, though all of whose 23 atoms is hard to be full-coincidently measured for the state of the art technique.[95] In the measurement, the difference between the interactions of left or right circularly polarized laser with molecules has been used to identify the chiral of samples. A recent study shows that the circularly polarized laser can induce a chiral fragmentation of a planar and thus a chiral molecule during its CE, in which the measured enantiomer structure from CEI strongly depends on the orientation of the molecule relative to the light propagation direction and the helicity of the ionizing light.[96] Furthermore, the CEI method has also been proven very successful in differentiating the conformational (geometric) isomers, like $C_2H_4Br_2$ and $C_6H_3F_2I$ molecules.[50,51,97]

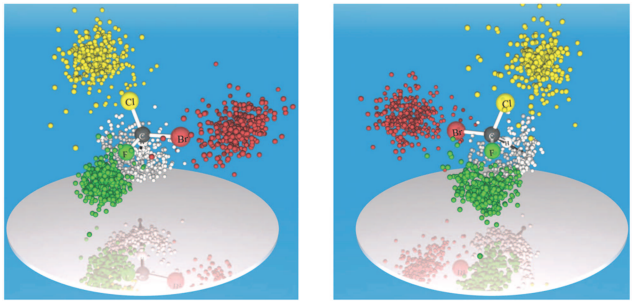


Fig. 12. Measured linear momenta in the fivefold fragmentation of two CHBrClF enantiomers, *i.e.*, (left) (S)-CHBrClF and (right) (R)-CHBrClF.[15]

4.2. Weakly-bound molecular clusters

Previously, the CEI has succeeded on obtaining the structures of atomic clusters,[98] the dimer formed by a molecule and an atom,[99,100] as well as molecular dimer.[53,55,56,101,102] Molecular clusters have complex structures and always with different isomers because of the weakly binding energies between their constitutive molecules. Imaging the structures of these molecular clusters is a challenge task for CEI due to their complicated interactions, multiple coexisted structures, and multi-body coincident measurement.

In the case of OCS dimer, there are four isomers with considerably different structures, *i.e.*, polar, nonpolar S-in, nonpolar O-in, and cross-shaped isomers. The four-body coincidence channels $(OCS)_2^{4+} \rightarrow CO^+ + S^+ + CO^+ + S^+$ have been used to identify these four isomers and determine their stereo configurations.[101] Though both the concerted and sequential fragmentations induced by the fs-laser fields are usually simultaneously measured in the experiment, only the event counts from the concerted process are selected, with the help of a classical trajectory simulation, for structural reconstruction. This can be achieved by examining the kinetic energy correlation maps of four CE fragments, where the experimental correlation diagrams exhibit two obvious regimes, marked by the red dashed circles and lines, respectively, as shown in Figs. 13(a1), 13(b1), and 13(c1), whereas the events from the sequential process distribute along the diagonal lines in the figures, indicating that two fragments share the same total energy available. The CCES results are also given out in the figure, in which the signal from concerted (sequential) fragmentation is shown in Figs. 13(a2), 13(b2) and 13(c2) [Figs. 13(a3), 13(b3), and 13(c3)]. In this way, the concerted and sequential events from the experimental measurement can be fully distinguished.

After the identification, a correlation map between $\theta_{CO+-CO+}$ and β can be given for the relative angular distribution ($\theta_{CO+-CO+}$, β) for the momenta of the four ions from concerted fragmentation as Fig. 14(a). As marked in the plots, there are three main regions, representing polar, nonpolar S-in, and cross-shaped structures, respectively. These multi-peak distributions in Figs. 14(b) and 14(c) can be well reproduced by performing the CCESs with three different structures of the dimers. The distributions for the angle β peak at 0°, 90°, and 180°, originating from the polar, cross-shaped, and nonpolar structures respectively.

Finally the stereo configurations of different isomers for $(OCS)_2$ are obtained through the reconstructions with the help of CCES as shown in Fig. 15. Furthermore, it is also demonstrated that the possible structures of other molecular clusters like CS_2 dimer and OCS cluster can be distinguished with the help of the combination of laser impulsive alignment and laser-induced CE.[55,56] These results show that the CEI presents great power in resolving the possible structures and imaging all the structures of molecular clusters directly.

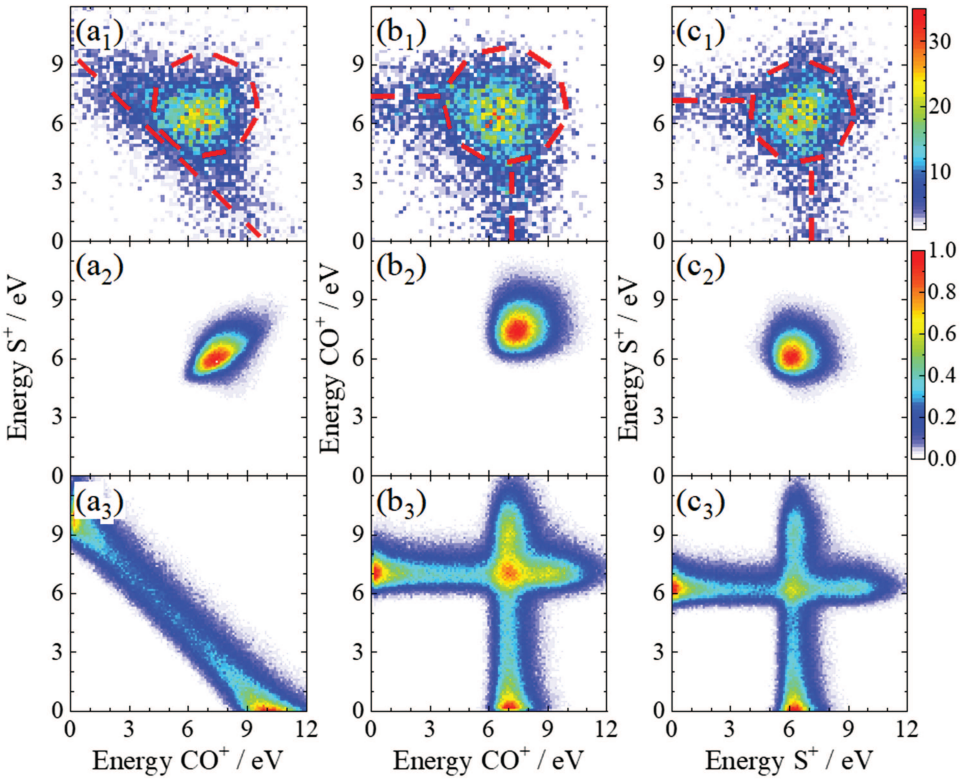


Fig. 13. Kinetic energy correlation maps for CO^+ and S^+: (a1)–(a3) for CO^+ *versus* S^+, (b1)–(b3) for CO^+ *versus* CO^+, and (c1)–(c3) for S^+ *versus* S^+. Panels (a1)–(c1) are the experimental data; panels (a2)–(c2) and (a3)–(c3) are the simulation results of the concerted and sequential processes for the nonpolar S-in isomer, respectively.[101]

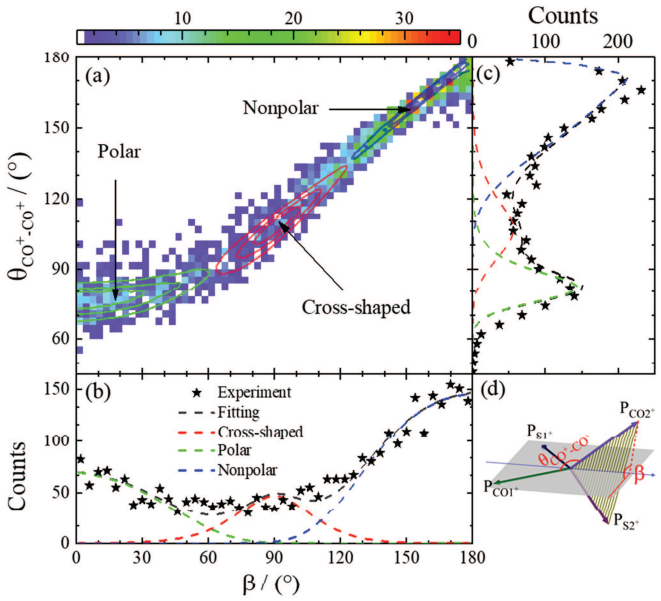


Fig. 14. (a) Correlation map distribution of $\theta_{CO+-CO+}$ and β for the concerted fragmentation events. Distribution of integrated angle (b) dihedral β and (c) $\theta_{CO+-CO+}$ for experiments (black stars) and simulations, along with the best fitting of the experiments according to simulations in black dashed lines. (d) The schematic diagram of the relative angles between momenta of fragments.[101]

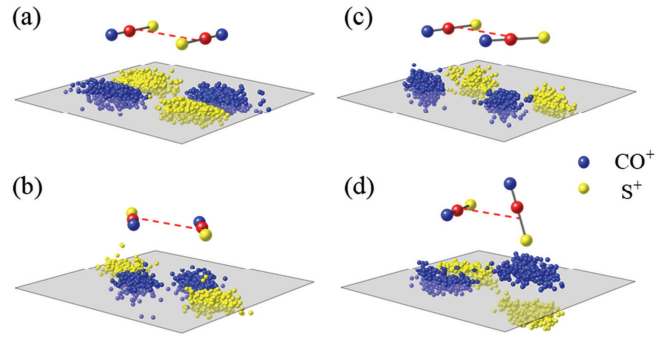


Fig. 15. The reconstructed geometries of the isomers and the corresponding predicted geometries shown as ball-and-stick models, (a) for nonpolar S-in, (b) for nonpolar O-in, (c) for polar, and (d) for cross-shaped isomers.[101]

In case of trimer, the stereo-configuration of molecular cluster containing benzene (Bz), *e.g.*, Bz_2Ar complex, can also be captured by femtosecond laser-induced CE.[103] Experimently, the momentum vectors of fragments from a femtosecond laser-induced three-body CE ($[Bz_2Ar]^{3+} \rightarrow Bz^+ + Bz^+ + Ar^+$) of Bz_2Ar are coincidently measured by the COLTRIMS setup. As shown by the measured Dalitz plot in Fig. 16(a), the distribution indicates that only a concerted fragmentation process occurs during the three-body CE of the Bz_2Ar, which may be attributed to the weak van der Waals interactions between the monomer molecules and atoms. As mentioned above, this analysis of dissociation process avoids the possible inaccuracy and unreliability of structural reconstruction induced by the sequential fragmentation.

The structure of the Bz_2Ar can be preliminarily determined by the relative momenta of the three ions by simulating the mapping between momentum and structure. As shown in Fig. 16(b), the measured result at coordinate (0, 0.12) give the relative angles between the momentum vectors of two Bz^+ about 125° and those of Bz^+ and Ar^+ about 117°. Since the mapping between momentum and structure is not unique, the momentum configuration can retrieve two potential candidate structures, (56°, 62°, 62°) and (120°, 30°, 30°), in the angle order of (∠Bz–Ar–Bz, ∠Ar–Bz–Bz, ∠Ar–Bz–Bz), by a point charge approximated CE simulation. And further quantum chemical computations are necessary to distinguish the two geometries.

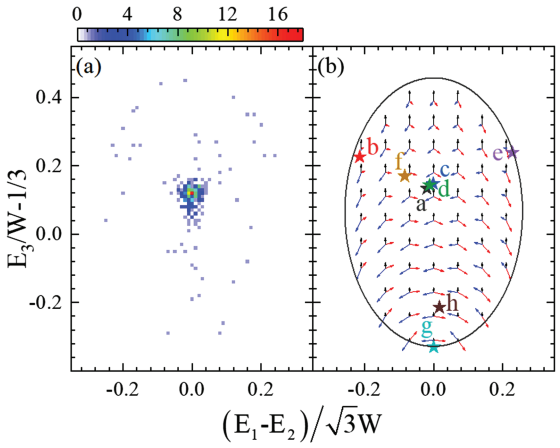


Fig. 16. (a) Dalitz plot of the events from three-body CE of Bz_2Ar, where E_1 and E_2 correspond to the kinetic energy of Bz^+, and E_3 corresponds to that of Ar^+. The distribution is centered at (0, 0.12). (b) Simulated positions of calculated isomers in the Dalitz plot and the relative momentum vector of the three ions are shown as arrows, red and blue for Bz and black for Ar.[103]

Figure 17 shows the optimized structures of the eight isomers of Bz_2Ar, showing mainly two types of isomers, triangularly distributed structure (in panels (a), (c), (d), (f)) and nearly linearly distributed structures (in panels (b), (e), (g), (h)). The relative angles among the center of mass of the constituents of Bz_2Ar show that the geometry of isomers (a), (c), and (d) are close to the structure (56°, 62°, 62°), and no isomer corresponds to the other preliminary candidate. This means that Bz_2Ar is probable to be a nearly equilateral triangular structure. The identification of structure is verified through a CCES of the three-body CE. Figure 16(b) presents the simulated positions of the eight optimized structures in the Dalits plot, which also indicates that the structure of Bz_2Ar is probable to be like (a), (c), and (d) isomers. The structure of Bz_2Ar can be reconstructed in coordinate space by fitting the simulated momenta to the measured ones for various initial structures using a genetic algorithm. The obtained values of bond length is only a little larger than that from quantum chemistry calculation, which may originate from the non-Coulomb effects, polarization between fragments, and the undetected internal energy during dissociation. Similarly to the trimer Bz_2Cu and Bz_2Zn, the triangular structures of Bz_2Ar system indicate that the interaction between Ar and Bz is very weak and the π–H interaction between two Bz molecules is dominant, due to the fully occupied valence orbitals of Ar. This work further shows

the potential of femtosecond laser-induced CE for imaging configuration of weakly bound molecular trimer.

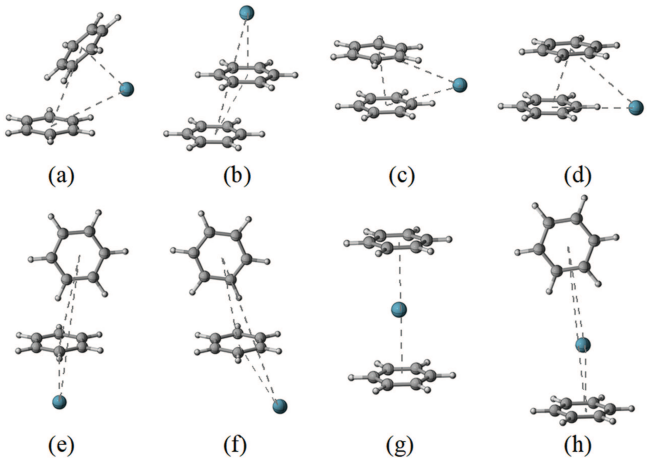


Fig. 17. The optimized structures of low-lying energy isomers of Bz_2Ar determined by M06-2X/6-311G(d), using the GAUSSIAN 09 package.[103]

It is worthy to note that the measured structural parameters, especially the atomic distance, are always larger than that from theoretical prediction. The discrepancies are induced by multiple factors during ionization and dissociation including the non-Coulomb effects between the explode spices[104] and laser-induced deformation, which lead the fragmentation process in experiment to be actually beyond the simple model of direct CE with Coulomb potential approximation. Furthermore, capturing the structures of complex molecules and molecular clusters are still limited by the detection efficiency during multiple-body coincidence measurements, though the five-body coincidence measurement for molecules, and four-body coincidence measurement for molecular cluster have been demonstrated successfully.[15,46,101] For imaging the structures of complex molecules and molecular clusters in the near future, increasing the detection efficiency and laser repetition rate, developing new correlation imaging methods, *i.e.* covariance and coincidence mapping method based on VMI images,[105,106] and combining the advanced laser manipulation molecules technology[49,95,107–109] are required.

5. Tracing the ultrafast structural evolution of molecules

Naturally, molecules often lie in a nonequilibrium or excited state, especially in the interaction with radiation, in the process of chemical reaction, or even in warm dense matters. Molecules become unstable when they absorb energy, and different quantum states can be populated selectively by photoexcitation,[10–13,18–23] which opens a door for quantum manipulation of molecular process in physical science. During the processes, bond breaking and visualizing nuclear movement of molecules play a vital role. This can be traced by a pump–probe method with the fs time scale resolution, which brings out the femto-chemistry. In the pump–probe method, the molecules are excited by the pump pulse and it triggers the dynamics along the potential energy surfaces as shown in Fig. 18. In the UCEI scheme, a strong probe pulse is used to ionize the excited molecules to their multi-charged states.[18–23] After that, the CE between the constitutive atoms/fragments are measured to reconstruct the structure at different delay times, representing the structural evolution. The ultrafast bond breaking, vibration, conical intersection, as well as roaming, have been imaged on the femtosecond time scale, thus, the molecular movies are presented.[18–23,52,87–90,110,111]

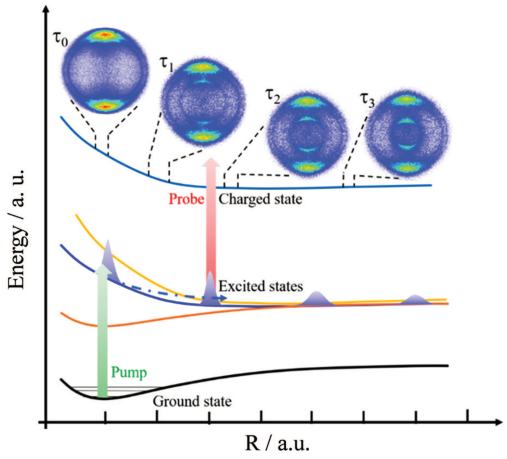


Fig. 18. The schematic diagram of UCEI. In the process, the pump laser first excites the molecule, and then a delayed probe laser further ionizes the excited molecule to multiply charged state and induces CE to track the nuclear evolution of samples.

It is well known that N_2O^+ is the intermediate product of the very important reaction $O^+ + N_2 \rightarrow NO^+ + N$ in the upper ionosphere of our earth.[112,113] Zhao *et al.* probed the ultrafast dissociation dynamics of N_2O cation and dictation by using a UCEI method.[21] The time-dependent three-body coincidence measurement ($N_2O^{3+} \rightarrow N^+ + N^+ + O^+$) reveals the ultrafast structural deformation and the dissociation of N_2O^+ and N_2O^{2+}. Figure 19(a) presents the measured time-dependent KER from the three-body CE channel. In the UCEI, the measured KER(t) $= E_0 + E_{\mathrm{Cou}}(t)$ (where $E_{\mathrm{Cou}}(t) = 1/R(t)$) is determined by the structure of the molecules when a probe laser arrives. Three bands can be resolved from the time-dependent KER spectra, in which the KER of two of them decreases as increasing the delay time. They come from the fast bond breaking of the molecular ions, and thus, the structure evolution after the molecular dissociation is further traced by coincidently measured momenta of three fragments, $N^+ + N^+ + O^+$. In this work, they have identified the dissociation with the momenta distribution of electrons as shown in Figs. 19(b) and 19(c). Since the targets are further probed by the elliptically polarized laser ($\varepsilon \sim 0.7$), the two peaks and three peaks distribution correspond to the cases of one electron and two electrons being ionized by the probe laser.[114–116]

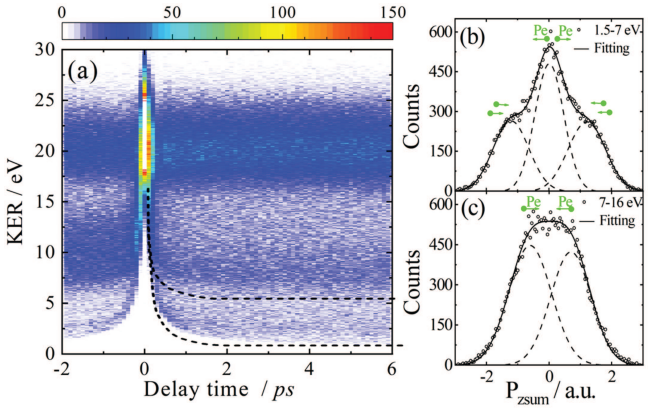


Fig. 19. (a) Pump–probe delay dependence of the KER for the three-body CE channel $N^+ + N^+ + O^+$ from further ionization of N_2O^+ and N_2O^{2+}. Two dashed lines are added to visualize the time dependence of KERs for two dissociation channels. Also shown are the corresponding ion sum-momentum distributions P_{zsum} for (b) the low-KER band (1.5 eV–7.0 eV) and (c) the high-KER band (7.0 eV–16.0 eV).[21]

This method makes the identification of the dissociation channel easier. The two-body and three-body dissociations from the $B^2\Pi$ state of N_2O^+ are tracked in real-time, furthermore, two two-body and two three-body fragmentation pathways are assigned with the help of energy correlation and time-resolved Dalitz plots for the ultrafast dissociation of N_2O^{2+}.

Another example is triatomic OCS molecules. The coupling between its cation states is found important in OCS^+ ultrafast dissociation.[22] Figure 20 gives the measured time-dependent KER from UCEI of OCS, in which the nuclear movement is tracked. For comparison, a theoretical calculation is performed based on the full calculation of PESs along with the semiclassical simulation considering the effect of Landau–Zener surface,[117] as shown in Figs. 20(c) and 20(d). In the low-KER channel from the direct three-body dissociation, the OCS^+ lies in the $3^2A''$ state after the ionization and then transfers to the $2^2A''$ state by a radial coupling, which can be treated as a direct breakup process. The high KER channel associated with both two-body and three-body dissociations is assigned to a sequential channel, in which the dissociation mainly starts from the $3^2A'$ state, and crosses the $4^2A'$ and $5^2A'$ states by an orbital overlapping and a conical intersection.

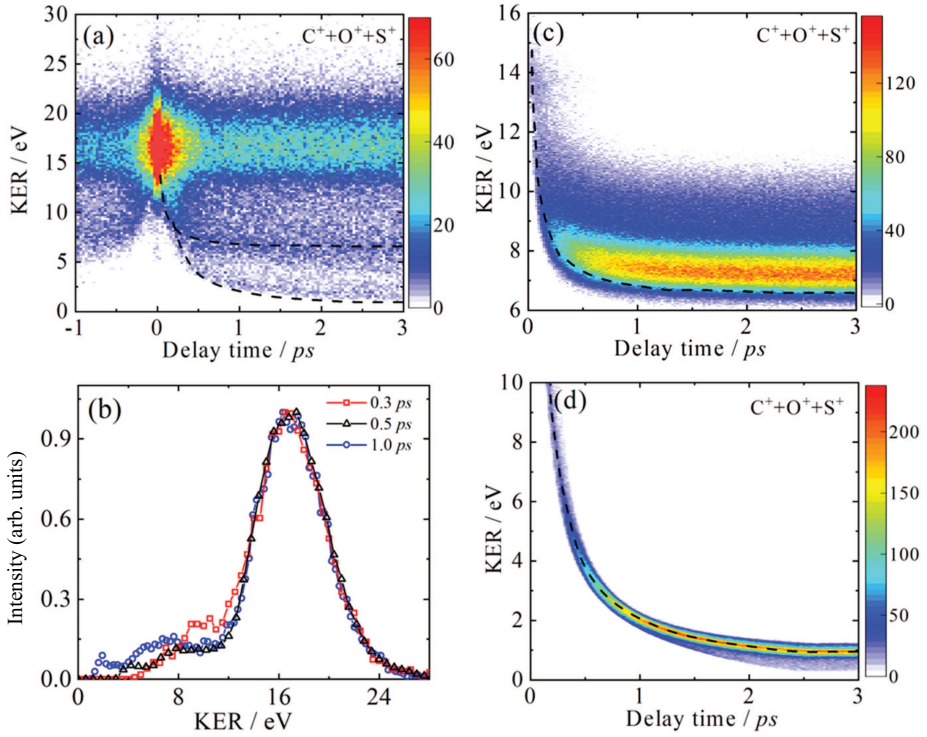


Fig. 20. (a) The measured time-dependent KER for the three-body CE channel $C^+ + O^+ + S^+$ of OCS molecule. (b) The integral KER spectra at three delay times (0.3, 0.5, and 1.0 ps) between pump–probe lasers. Panels (c) and (d) are the calculated time-dependent KER from sequential dissociation pathway and direct three-body fragmentation pathway.[22]

The coupling between excitation states is important during the ultrafast conical intersection between $^3Q_0$ and $^1Q_1$ states of CH_3I,[87] which are tracked by ionizing the molecules to dictation states and measuring the time-resolved KER from CE channel $CH_3^+ + I^+$. The corresponding evolutions along different states have been identified by performing the surface-hopping trajectory calculations. The UCEI has been also widely used to capture the H migration process of charged hydrocarbon molecules, both the single and double H migration have been observed in real-time.[118] Furthermore, the corresponding roaming dynamics have been proposed and captured in the time-resolved measurement.[52,90] Recently, the other case has been published in *science*, in which they directly imaged individual "roamers" on ultrafast time scales in

the prototypical formaldehyde dissociation reaction by using UCEI. In the experiment, the D_2CO molecules are excited to $\tilde{A}$ state and trigger the roaming dynamics by absorbing one 304-nm photon, and another strong laser (800 nm, 8 fs) ionizes the molecules to the trication state and induces the CE of molecules.[52] The time-dependent three-body breakup fragments, $D^+ + D^+ + CO^+$, are measured, and the time evolution of the experimental KER *versus* deuteron momentum angle representation shows the evidence of roaming contribution of molecules, as given in Fig. 21. Therefore, the real-time roaming dynamics of D_2CO are captured on the fs time scale and Å spatial scale with the help of high-level first-principles simulations.

The UCEI can also be used to study the neighbor effect in fragmentation of cluster on femtosecond timescale. Recently, we perform a time-resolved study on tracking the neighbor roles in the fragmentation of N_2O molecules in a dimer.[119] In experiment, the time-dependent three-body CE channel ($N^+ + NO^+ + N_2O^+$) is measured coincidently. With the help of calculated PECs by the complete active space self-consistent field (CASSCF) method, the results show that the existence of neighbor molecule or molecular ion will induce the rotation of molecules during fragmentation. A fast rotation of N_2O^+ is observed when the neighbor is a molecular ion and the rotation is slower when the neighbor is a neutral molecule. The existence of a neighbor ion changes the yield ratio of products by modifying the parity of states during molecular dissociation due to the spin-exchange effect, which open new dissociation channel of molecules and leads to the formation of metastable products $N_3O_2^+$ from the ion–molecule collision. These observations through UCEI contribute a significant step to understanding of the neighbor effect on the fragmentation of molecular clusters.

These studies demonstrated the great power of UCEI on the complex dynamics of polyatomic molecules. However, the study of ultrafast dynamics of the molecular clusters through UCEI is still very limited since the difficulty in both the experiments and theories.[111,120,121] In the molecular cluster, the reaction between molecules or the environmental effects becomes important. It suggests that tracking the ultrafast dynamics not only will promote our understanding of the dissociation or formation of clusters but also pave the way to control the reaction between molecules. Thus, it is reasonable to believe that tracking the ultrafast dynamics of the molecular clusters will capture great attention in the ultrafast science community.

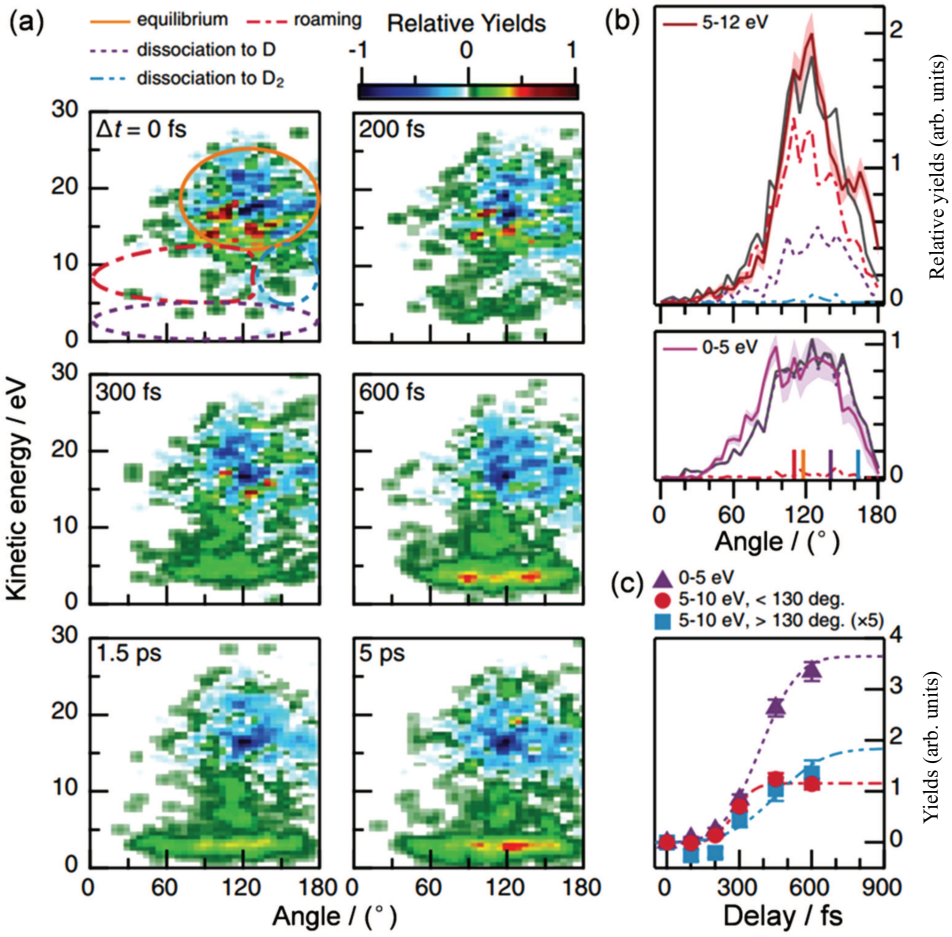


Fig. 21. Experimental results of the three-body breakup (D^+, D^+, CO^+) channel after pumped by a 304-nm photon. (a) and (b) Time-integrated angular distribution of deuteron momenta for the experiment (red and purple solid lines) and molecular dynamics simulations. (c) Yields of selected KER and angular regions as a function of time delay.[52]

6. Summary

Laser-induced CEI presents a great ability to image the static stereo configurations of small molecules and molecular clusters, and it can also be extended to track the ultrafast dynamics of these systems with the help of the pump–probe method. This ultrafast measurement technique requires multiple ionization of samples, which can capture the structure of molecules and clusters with Å spatial and fs temporal resolution. However, due to the complex dynamics in molecular fragmentation, the correct structural reconstruction also relies on the full understanding of the ionization and dissociation dynamics during the strong laser interaction with molecules and clusters. The exemplary previous results show that the structures, the chiral configurations, and the conformation of molecules and molecular clusters can be imaged and determined. With the UCEI method, the dissociation dynamics, the conical intersection between excitation states, and the complex roaming dynamics of molecules can be tracked on the fs time scale. Furthermore, combined with the laser alignment technique as well as developing new imaging techniques, the UCEI method can be extended to more complex molecules and molecular clusters, which further give more opportunity to study the environmental effects on ultrafast dissociation of small quantum systems. The development of FEL in recent years also promotes the combination of fs FEL and CEI being a promising atomic-resolution imaging tool, whose key advantage lies in the ease of creating very high charge states within a few femtoseconds.[47] More applications of FEL-induced CEI integrated with two-color or time-resolved pump–probe method is expected to be achieved in the near future,[122] which benefit from the shorter and shorter pulse durations and increasing repetition rates of FELs nowadays. In general, the combination of CEI techniques with state-of-the-art theoretical toolkits will further deepen our fundamental understanding of chemical reactivity and chemical bonding, and achieve the dream of making ultrafast time-resolved molecular movies.

Acknowledgements

Project partially supported by the National Key Research and Development Program of China (Grant Nos. 2019YFA0307700), the National Natural Science Foundation of China (Grant Nos. 12004133, 12074143, 12134005, and 11904210), and China Postdoctoral Science Foundation (Grant No. 2021M691220).

References

[1] Peplow M 2017 *Nature* **544** 408
[2] Neutze R, Wouts R, van der Spoel D, Weckert E and Hajdu J 2000 *Nature* **406** 752
[3] Ihee H, Lorenc M, Kim T K, Kong Q Y, Cammarata M, Lee J H, Bratos S and Wulff M 2005 *Science* **309** 1223
[4] Gaffney K J and Chapman H N 2007 *Science* **316** 1444
[5] Gross L, Mohn F, Moll N, Liljeroth P and Meyer G 2009 *Science* **325** 1110
[6] Suzuki S, Green P G, Bumgarner R E, Dasgupta S, Goddard W A and Blake G A 1992 *Science* **257** 942
[7] Zhang B, Yu Y, Zhang Y Y, Jiang S, Li Q, Hu H S, Li G, Zhao Z, Wang C, Xie H, Zhang W, Dai D, Wu G, Zhang D H, Jiang L, Li J and Yang X 2020 *Proc. Nat. Acad. Sci.* **117** 15423
[8] Li G, Zhang Y Y, Li Q, Wang C, Yu Y, Zhang B, Hu H S, Zhang W, Dai D, Wu G, Zhang D H, Li J, Yang X and Jiang L 2020 *Nat. Commun.* **11** 5449
[9] Li J, Li X, Zhai H J and Wang L S 2003 *Science* **299** 864
[10] Glownia J M, Natan A, Cryan J P, Hartsock R, Kozina M, Minitti M P, Nelson S, Robinson J, Sato T, van Driel T, Welch G, Weninger C, Zhu D and Bucksbaum P H 2016 *Phys. Rev. Lett.* **117** 153003
[11] Yang J, Guehr M, Shen X, Li R, Vecchione T, Coffee R, Corbett J, Fry A, Hartmann N, Hast C, Hegazy K, Jobe K, Makasyuk I, Robinson J, Robinson M S, Vetter S, Weathersby S, Yoneda C, Wang X and Centurion M 2016 *Phys. Rev. Lett.* **117** 153002
[12] Yang J, Zhu X, Wolf Thomas J A, Li Z, Nunes J P F, Coffee R, Cryan James P, Gühr M, Hegazy K, Heinz Tony F, Jobe K, Li R, Shen X, Veccione T, Weathersby S, Wilkin Kyle J, Yoneda C, Zheng Q, Martinez Todd J, Centurion M and Wang X 2018 *Science* **361** 64
[13] Yang J, Zhu X, Pedro F N J, Yu Jimmy K, Parrish Robert M, Wolf Thomas J A, Centurion M, Gühr M, Li R, Liu Y, Moore B, Niebuhr M, Park S, Shen X, Weathersby S, Weinacht T, Martinez Todd J and Wang X 2020 *Science* **368** 885
[14] Vager Z, Naaman R and Kanter E P 1989 *Science* **244** 426
[15] Pitzer M, Kunitski M, Johnson A S, Jahnke T, Sann H, Sturm F, Schmidt L P H, Schmidt-Böcking H, Dörner R, Stohner J, Kiedrowski J, Reggelin M, Marquardt S, Schießer A, Berger R and Schöffler M S 2013 *Science* **341** 1096
[16] Herwig P, Zawatzky K, Grieser M, Heber O, Jordon-Thaden B, Krantz C, Novotny O, Repnow R, Schurig V, Schwalm D, Vager Z, Wolf A, Trapp O and Kreckel H 2013 *Science* **342** 1084
[17] Stapelfeldt H, Constant E and Corkum P B 1995 *Phys. Rev. Lett.* **74** 3780
[18] Bocharova I A, Alnaser A S, Thumm U, Niederhausen T, Ray D, Cocke C L and Litvinyuk I V 2011 *Phys. Rev. A* **83** 013417
[19] Jiang Y H, Rudenko A, Herrwerth O, Foucar L, Kurka M, Kühnel K U, Lezius M, Kling M F, van Tilborg J, Belkacem A, Ueda K, Düsterer S, Treusch R, Schröter C D, Moshammer R and Ullrich J 2010 *Phys. Rev. Lett.* **105** 263002
[20] Lin K, Hu X, Pan S, Chen F, Ji Q, Zhang W, Li H, Qiang J, Sun F, Gong X, Li H, Lu P, Wang J, Wu Y and Wu J 2020 *J. Phys. Chem. Lett.* **11** 3129
[21] Zhao X, Yu X, Xu X, Yin Z, Yu J, Li X, Ma P, Zhang D, Wang C, Luo S and Ding D 2020 *Phys. Rev. A* **101** 013416
[22] Zhao X, Xu T, Yu X, Ren D, Zhang X, Li X, Ma P, Wang C, Zhang D, Wang Q, Hu X, Luo S, Wu Y, Wang J and Ding D 2021 *Phys. Rev. A* **103** 053103
[23] Li M, Zhang M, Vendrell O, Guo Z, Zhu Q, Gao X, Cao L, Guo K, Su Q Q, Cao W, Luo S, Yan J, Zhou Y, Liu Y, Li Z and Lu P 2021 *Nat. Commun.* **12** 4233
[24] Dahl P F, Costello D G and Walters W L 1960 *Nucl. Phys.* **21** 106
[25] Breskin A, Faibis A, Goldring G, Hass M, Kaim R, Vager Z and Zwang N 1979 *Phys. Rev. Lett.* **42** 369
[26] Gemmell D S 1980 *Chem. Rev.* **80** 301
[27] Yatsuhashi T and Nakashima N 2018 *J. Photochem. Photobiol., C* **34** 52
[28] Vager Z, Kanter E P, Both G, Cooney P J, Faibis A, Koenig W, Zabransky B J and Zajfman D 1986 *Phys. Rev. Lett.* **57** 2793
[29] Plesser I, Vager Z and Naaman R 1986 *Phys. Rev. Lett.* **56** 1559
[30] Zhu Z S, Miao J W, Liao X H, Miao L, Yuan X D and Shi M G 2009 *Chin. Phys. B* **18** 4840
[31] Frasinski L J, Codling K, Hatherly P, Barr J, Ross I N and Toner W T 1987 *Phys. Rev. Lett.* **58** 2424
[32] Cornaggia C, Lavancier J, Normand D, Morellec J, Agostini P, Chambaret J P and Antonetti A 1991 *Phys. Rev. A* **44** 4499
[33] Strickland D T, Beaudoin Y, Dietrich P and Corkum P B 1992 *Phys. Rev. Lett.* **68** 2755
[34] Codling K and Frasinski L J 1993 *J. Phys. B* **26** 783

[35] Codling K and Frasinski L J 1994 *Contemp. Phys.* **35** 243
[36] Posthumus J H 2004 *Rep. Prog. Phys.* **67** 623
[37] Stapelfeldt H, Constant E, Sakai H and Corkum P B 1998 *Phys. Rev. A* **58** 426
[38] Frasinski L J, Codling K and Hatherly P A 1989 *Science* **246** 1029
[39] Schouder C A, Chatterley A S, Pickering J D and Stapelfeldt H 2022 *Annu. Rev. Phys. Chem.* **73** 323
[40] Eppink A T J B and Parker D H 1997 *Rev. Sci. Instrum.* **68** 3477
[41] Dörner R, Mergel V, Jagutzki O, Spielberger L, Ullrich J, Moshammer R and Schmidt-Böcking H 2000 *Phys. Rep.* **330** 95
[42] Ullrich J, Moshammer R, Dorn A, Dörner R, Schmidt L P H and Schmidt-Böcking H 2003 *Rep. Prog. Phys.* **66** 1463
[43] Hasegawa H, Hishikawa A and Yamanouchi K 2001 *Chem. Phys. Lett.* **349** 57
[44] Hishikawa A, Hasegawa H and Yamanouchi K 2002 *Chem. Phys. Lett.* **361** 245
[45] Légaré F, Lee K F, Litvinyuk I V, Dooley P W, Wesolowski S S, Bunker P R, Dombi P, Krausz F, Bandrauk A D, Villeneuve D M and Corkum P B 2005 *Phys. Rev. A* **71** 013415
[46] Pitzer M 2017 *J. Phys. B* **50** 153001
[47] Boll R, Schäfer J M, Richard B, Fehre K, Kastirke G, Jurek Z, Schöffler M S, Abdullah M M, Anders N, Baumann T M, Eckart S, Erk B, De Fanis A, Dörner R, Grundmann S, Grychtol P, Hartung A, Hofmann M, Ilchen M, Inhester L, Janke C, Jin R, Kircher M, Kubicek K, Kunitski M, Li X, Mazza T, Meister S, Melzer N, Montano J, Music V, Nalin G, Ovcharenko Y, Passow C, Pier A, Rennhack N, Rist J, Rivas D E, Rolles D, Schlichting I, Schmidt L P H, Schmidt P, Siebert J, Strenger N, Trabert D, Trinter F, Vela-Perez I, Wagner R, Walter P, Weller M, Ziolkowski P, Son S K, Rudenko A, Meyer M, Santra R and Jahnke T 2022 *Nat. Phys.* **18** 423
[48] Ma L, Yong H, Geiser J D, Moreno Carrascosa A, Goff N and Weber P M 2020 *Struct. Dynam.* **7** 034102
[49] Luo S, Zhu R, He L, Hu W, Li X, Ma P, Wang C, Liu F, Roeterdink W G, Stolte S and Ding D 2015 *Phys. Rev. A* **91** 053408
[50] Ablikim U, Bomme C, Xiong H, Savelyev E, Obaid R, Kaderiya B, Augustin S, Schnorr K, Dumitriu I, Osipov T, Bilodeau R, Kilcoyne D, Kumarappan V, Rudenko A, Berrah N and Rolles D 2016 *Sci. Rep.* **6** 38202
[51] Burt M, Amini K, Lee J W L, Christiansen L, Johansen R R, Kobayashi Y, Pickering J D, Vallance C, Brouard M and Stapelfeldt H 2018 *J. Chem. Phys.* **148** 091102
[52] Endo T, Neville Simon P, Wanie V, Beaulieu S, Qu C, Deschamps J, Lassonde P, Schmidt Bruno E, Fujise H, Fushitani M, Hishikawa A, Houston Paul L, Bowman Joel M, Schuurman Michael S, Légaré F and Ibrahim H 2020 *Science* **370** 1072
[53] Khan A, Jahnke T, Zeller S, Trinter F, Schöffler M, Schmidt L P H, Dörner R and Kunitski M 2020 *J. Phys. Chem. Lett.* **11** 2457
[54] Zhu X, Hu X, Yan S, Peng Y, Feng W, Guo D, Gao Y, Zhang S, Cassimi A, Xu J, Zhao D, Dong D, Hai B, Wu Y, Wang J and Ma X 2020 *Nat. Commun.* **11** 2987
[55] Pickering J D, Shepperson B, Christiansen L and Stapelfeldt H 2018 *J. Chem. Phys.* **149** 154306
[56] Pickering J D, Shepperson B, Hübschmann B A K, Thorning F and Stapelfeldt H 2018 *Phys. Rev. Lett.* **120** 113202
[57] Niikura H, Légaré F, Hasbani R, Ivanov M Y, Villeneuve D M and Corkum P B 2003 *Nature* **421** 826
[58] Wang E, Shan X, Shen Z, Li X, Gong M, Tang Y and Chen X 2015 *Phys. Rev. A* **92** 062713
[59] Wang Y, Shi X, Zhou J, Xu S, Guo D, Yan S, Zhu X and Ma X 2020 *Phys. Rev. A* **101** 042706
[60] Wang B, Han J, Zhu X, Wei L, Ren B, Zhang Y, Yu W, Yan S, Ma X, Zou Y, Chen L and Wei B 2021 *Phys. Rev. A* **103** 042810
[61] Zhao X, Shan X, Zhu X, Chen L, Shen Z, Feng W, Guo D, Zhao D, Zhang R, Gao Y, Huang Z, Zhang S, Ma X and Chen X 2021 *Chin. Phys. B* **30** 113302
[62] Zhang M, Najjari B, Hai B, Zhao D M, Lei J T, Dong D P, Zhang S F and Ma X W 2020 *Chin. Phys. B* **29** 063302
[63] Wu C, Wu C, Song D, Su H, Yang Y, Wu Z, Liu X, Liu H, Li M, Deng Y, Liu Y, Peng L Y, Jiang H and Gong Q 2013 *Phys. Rev. Lett.* **110** 103601
[64] Ma J, Lin K, Ji Q, Zhang W, Li H, Sun F, Qiang J, Lu P, Li H, Gong X and Wu J 2019 *Chin. Phys. B* **28** 093301
[65] Liu H, Li M, Xie X G, Wu C, Deng Y K, Wu C Y, Gong Q H and Liu Y Q 2015 *Chin. Phys. Lett.* **32** 063301
[66] Ma P, Wang C, Li X, Yu X, Tian X, Hu W, Yu J, Luo S and Ding D 2017 *J. Chem. Phys.* **146** 244305
[67] Ma P, Wang C, Luo S, Yu X, Li X, Wang Z, Hu W, Yu J, Yang Y, Tian X, Cui Z and Ding D 2018 *J. Phys. B* **51** 094002
[68] Ma P, Wang C, Luo S, Li X, Hu W, Yu J, Yu X, Tian X, Qu Z and Ding D 2019 *Phys. Rev. A* **99** 023423
[69] Zhang D, Luo S, Xu H, Jin M, Liu F, Yan B, Wang Z, Liu H, Jiang D, Eppink A, Roeterdink W, Stolte S and Ding D 2017 *Eur. Phys. J. D* **71** 148
[70] Luo S, Hu W, Yu J, Li X, He L, Wang C, Liu F and Ding D 2017 *J. Phys. Chem. A* **121** 6547
[71] Luo S, Zhou S, Hu W, Yu J, Li X, Ma P, He L, Wang C, Guo F, Yang Y and Ding D 2018 *J. Phys. Chem. A* **122** 8427
[72] Wang X, Zhang J, Zhang S A and Sun Z R 2016 *Chin. Phys. B* **25** 53301
[73] Li H Y, Huang M D, Kang M and Li D J 2018 *Chin. Phys. B* **27** 63602
[74] Li X, Ren H Z, Ma R, Chen J X, Yang H and Gong Q H 2005 *Chin. Phys. B* **13** 1564
[75] Hu X, Peng Y, Zhu X, Yan S, Liu L, Feng W, Guo D, Gao Y, Zhang S, Zhao D, Dong D, Hai B, Xu J, Zhang S, Ma X, Wang J and Wu Y 2020 *Phys. Rev. A* **101** 012707
[76] Luzon I, Livshits E, Gope K, Baer R and Strasser D 2019 *J. Phys. Chem. Lett.* **10** 1361
[77] Zhou W, Ge L, Cooper G A, Crane S W, Evans M H, Ashfold M N R and Vallance C 2020 *J. Chem. Phys.* **153** 184201
[78] Hishikawa A, Iwamae A and Yamanouchi K 1999 *Phys. Rev. Lett.* **83** 1127
[79] Sato Y, Kono H, Koseki S and Fujimura Y 2003 *J. Am. Chem. Soc.* **125** 8019
[80] Hansen J L, Nielsen J H, Madsen C B, Lindhardt A T, Johansson M P, Skrydstrup T, Madsen L B and Stapelfeldt H 2012 *J. Chem. Phys.* **136** 204310
[81] Rajput J, Severt T, Berry B, Jochim B, Feizollah P, Kaderiya B, Zohrabi M, Ablikim U, Ziaee F, Raju P K, Rolles D, Rudenko A, Carnes K D, Esry B D and Ben-Itzhak I 2018 *Phys. Rev. Lett.* **120** 103001
[82] Alnaser A S, Tong X M, Osipov T, Voss S, Maharjan C M, Ranitovic P, Ulrich B, Shan B, Chang Z, Lin C D and Cocke C L 2004 *Phys. Rev. Lett.* **93** 183202
[83] Hanus V, Kangaparambil S, Larimian S, Dorner-Kirchner M, Xie X, Schöffler M S, Paulus G G, Baltuška A, Staudte A and Kitzler-Zeiler M 2020 *Phys. Rev. Lett.* **124** 103201
[84] Hering P and Cornaggia C 1999 *Phys. Rev. A* **59** 2836
[85] Bryan W A, Sanderson J H, El-Zein A, Newell W R, Taday P F and Langley A J 2000 *J. Phys. B* **33** 745
[86] Shi H T and Miao X Y 2013 *Chin. Phys. Lett.* **30** 063101
[87] Corrales M E, González-Vázquez J, de Nalda R and Bañares L 2019 *J. Phys. Chem. Lett.* **10** 138
[88] Xu H, Okino T and Yamanouchi K 2009 *J. Chem. Phys.* **131** 151102
[89] Xu H, Marceau C, Nakai K, Okino T, Chin S L and Yamanouchi K 2010 *J. Chem. Phys.* **133** 071103
[90] Ekanayake N, Severt T, Nairat M, Weingartz N P, Farris B M, Kaderiya B, Feizollah P, Jochim B, Ziaee F, Borne K, Raju P K, Carnes K D, Rolles D, Rudenko A, Levine B G, Jackson J E, Ben-Itzhak I and Dantus M 2018 *Nat. Commun.* **9** 5186
[91] Sanderson J H, El-Zein A, Bryan W A, Newell W R, Langley A J and Taday P F 1999 *Phys. Rev. A* **59** R2567
[92] Hishikawa A, Iwamae A, Hoshina K, Kono M and Yamanouchi K 1998 *Chem. Phys. Lett.* **282** 283
[93] Bocharova I, Karimi R, Penka E F, Brichta J P, Lassonde P, Fu X, Kieffer J C, Bandrauk A D, Litvinyuk I, Sanderson J and Légaré F 2011 *Phys. Rev. Lett.* **107** 063201
[94] Chen J X, Ma R, Ren H Z, Li X, Yang H and Gong Q H 2003 *Chin. Phys. Lett.* **20** 1040
[95] Christensen L, Nielsen J H, Slater C S, Lauer A, Brouard M and Stapelfeldt H 2015 *Phys. Rev. A* **92** 033411
[96] Fehre K, Eckart S, Kunitski M, Pitzer M, Zeller S, Janke C, Trabert D, Rist J, Weller M, Hartung A, Schmidt L P H, Jahnke T, Berger R, Dörner R and Schöffler M S 2019 *Sci. Adv.* **5** eaau7923
[97] Pathak S, Obaid R, Bhattacharyya S, Bürger J, Li X, Tross J, Severt T, Davis B, Bilodeau R C, Trallero-Herrero C A, Rudenko A, Berrah N and Rolles D 2020 *J. Phys. Chem. Lett.* **11** 10205

[98] Ulrich B, Vredenborg A, Malakzadeh A, Schmidt L P H, Havermeier T, Meckel M, Cole K, Smolarski M, Chang Z, Jahnke T and Dörner R 2011 *J. Phys. Chem. A* **115** 6936

[99] Wu J, Kunitski M, Schmidt L P H, Jahnke T and Dörner R 2012 *J. Chem. Phys.* **137** 104308

[100] Wu C, Wu C, Song D, Su H, Xie X, Li M, Deng Y, Liu Y and Gong Q 2014 *J. Chem. Phys.* **140** 141101

[101] Yu X, Zhao X, Wang Z, Yang Y, Zhang X, Ma P, Li X, Wang C, Xu X, Wang C, Zhang D, Luo S and Ding D 2021 *Phys. Rev. A* **104** 053104

[102] Song P, Wang X, Meng C, Dong W, Li Y, Lv Z, Zhang D, Zhao Z and Yuan J 2019 *Phys. Rev. A* **99** 053427

[103] Yu X, Liu Y, Deng K, Zhang X, Ma P, Li X, Wang C, Cui Z, Luo S and Ding D 2022 *Phys. Rev. A* **105** 063105

[104] Schouder C A, Chatterley A S, Madsen L B, Jensen F and Stapelfeldt H 2020 *Phys. Rev. A* **102** 063125

[105] Slater C S, Blake S, Brouard M, Lauer A, Vallance C, Bohun C S, Christensen L, Nielsen J H, Johansson M P and Stapelfeldt H 2015 *Phys. Rev. A* **91** 053424

[106] Vallance C, Heathcote D and Lee J W L 2021 *J. Phys. Chem. A* **125** 1117

[107] Christensen L, Christiansen L, Shepperson B and Stapelfeldt H 2016 *Phys. Rev. A* **94** 023410

[108] Saribal C, Owens A, Yachmenev A and Küpper J 2021 *J. Chem. Phys.* **154** 071101

[109] Luo S, Hu W, Yu J, Zhu R, He L, Li X, Ma P, Wang C, Liu F, Roeterdink W G, Stolte S and Ding D 2017 *J. Phys. Chem. A* **121** 777

[110] Zhou J, He C, Liu M M, Wang E, Jia S, Dorn A, Ren X and Liu Y 2021 *Phys. Rev. Res.* **3** 023050

[111] Wang E, Ren X and Dorn A 2021 *Phys. Rev. Lett.* **126** 103402

[112] Burley J D, Ervin K M and Armentrout P B 1987 *J. Chem. Phys.* **86** 1944

[113] Smith D R, Huppi E R and Wise J O 2000 *J. Atmos. Sol.-Terr. Phys.* **62** 1189

[114] Eckle P, Smolarski M, Schlup P, Biegert J, Staudte A, Schöffler M, Muller H G, Dörner R and Keller U 2008 *Nat. Phys.* **4** 565

[115] Pfeiffer A N, Cirelli C, Smolarski M, Dörner R and Keller U 2011 *Nat. Phys.* **7** 428

[116] Luo S, Liu J, Li X, Zhang D, Yu X, Ren D, Li M, Yang Y, Wang Z, Ma P, Wang C, Zhao J, Zhao Z and Ding D 2021 *Phys. Rev. Lett.* **126** 103202

[117] Belyaev A K, Domcke W, Lasser C and Trigila G 2015 *J. Chem. Phys.* **142** 104307

[118] Kling N G, Díaz-Tendero S, Obaid R, Disla M R, Xiong H, Sundberg M, Khosravi S D, Davino M, Drach P, Carroll A M, Osipov T, Martín F and Berrah N 2019 *Nat. Commun.* **10** 2813

[119] Yu X, Zhang X, Hu X, Zhao X, Ren D, Li X, Ma P, Wang C, Wu Y, Luo S and Ding D 2022 *Phys. Rev. Lett.* **129** 023001

[120] Wang E, Ren X, Baek W, Rabus H, Pfeifer T and Dorn A 2020 *Nat. Commun.* **11** 2194

[121] Ren X, Zhou J, Wang E, Yang T, Xu Z, Sisourat N, Pfeifer T and Dorn A 2022 *Nat. Chem.* **14** 232

[122] Picón A, Lehmann C S, Bostedt C, Rudenko A, Marinelli A, Osipov T, Rolles D, Berrah N, Bomme C, Bucher M, Doumy G, Erk B, Ferguson K R, Gorkhover T, Ho P J, Kanter E P, Krässig B, Krzywinski J, Lutman A A, March A M, Moonshiram D, Ray D, Young L, Pratt S T and Southworth S H 2016 *Nat. Commun.* **7** 11652